A method for computing calibrated ocean wave spectra from measurements with a nautical X-band radar

Conference Paper · November 1997

DOI: 10.1109/OCEANS.1997.624154 · Source: IEEE Xplore

3 authors, including:

Joerg Seemann
Helmholtz-Zentrum Hereon
69 PUBLICATIONS **899** CITATIONS
SEE PROFILE

Christian Senet
Bundesamt für Seeschifffahrt und Hydrographie
37 PUBLICATIONS **551** CITATIONS
SEE PROFILE

A Method for Computing Calibrated Ocean Wave Spectra from Measurements with a Nautical X-Band Radar

Jörg Seemann, Friedwart Ziemer, Christian M. Senet

GKSS Forschungszentrum Geesthacht
Max-Planck-Str., D-21502 Geesthacht, Germany
phone: + 49 4152 87 1567 , fax: + 49 4152 87 1565
e-mail: Seemann@gkss.de

Abstract

The radar backscatter from the ocean surface, called sea clutter, is modulated due to the surface wave field. The modulation introduces a spatio-temporal correlation of the sea clutter signal. A three-dimensional wavenumber frequency spectrum of the sea clutter is calculated from a time series of radar images with an FFT algorithm. Because of the non-linearity of the imaging process the image spectrum contains harmonics in addition to the linear fundamental mode. These modes are localized at distinct surfaces in the wave number frequency space corresponding to the scaled dispersion relation of surface gravity waves. Because of the localization of the spectral energy on dispersion shells, the aliasing effect due to a temporal undersampling can be overcome. The dispersion shells are reconstructed over the Nyquist frequency barrier and for negative frequencies. The dispersion shells are used as spectral filters to separate the modes from the clutter noise pedestal of radar image spectra. This pedestal shows the effect of the impulse response due to the finite spatial resolution of the radar. The spectral energy of the wavenumber frequency spectrum is integrated over the frequency coordinate axis, with the positive solution of the dispersion relation of surface gravity waves as signal filter. With this spectral filter method an unambiguous wave number image spectrum is selected. The fundamental image spectrum is related to the surface wave spectrum by an image transfer function. An empirical calibration procedure is presented. This procedure is based on the correlation of the signal to noise ratio with the significant wave height. The applicability of the method is shown using a radar and buoy data set. The spectral energies of fundamental mode, first harmonic, and the clutter component are compared. It was proved that the spectral energy of the clutter noise exceeds the spectral energy of the first harmonic mode by an order of magnitude, i.e. the physical background of the empirical calibration method is similar to the method well established for wave spectra from single SAR images.

1 Introduction

The backscatter of microwaves from the ocean surface is observable on the screen (Plan Position Indicator, PPI) of a nautical radar as sea clutter. *Young et al.* [1985] showed that it is possible to use a nautical radar to extract spectral information about the ocean surface wave field from the modulated sea clutter. A combined hardware [*Dittmer*, 1995] /software [*Ziemer*, 1995] system called WaMoS (Wave Monitoring System) was developed at the GKSS research center. This system enables calculation of surface wave spectra and the near surface current from sampled video signals of a commercial nautical radar. This system has been proved to be reliable for offshore applications [*Magnusson*, 1995] and at the Spanish coast [*Nieto Borge*, 1995]. The standard method has certain limitations for measuring short waves, especially when the radar is used from a moving platform. However these waves are imaged by the radar. The task was to overcome these limitations using an improved understanding of structure of the wavenumber frequency spectrum calculated from the spatio-temporal sea clutter signal.

2 Sea Clutter

In contrast to airplane- and satellite-mounted radars, the nautical radar images the ocean surface at grazing incidence. Recent measurements at grazing incidence by *Lee et al.* [1995] indicate that the backscatter for HH-polarization, used by commercial nautical radars, results from small scale breaking waves as scattering elements.
The ocean wave field is imaged with the radar because the waves modulate the radar cross section of the ocean surface. At moderate incidence angles tilt- and hydrodynamic modulation are well established imaging mechanisms [*Alpers et al.*, 1981]. For grazing angles less than the slope of the ocean waves, shadowing occurs, resulting in an additional strong modulation of the radar images. Shadowing is assumed to be the main imaging mechanism at grazing incidence.
Ward et al. [1990] observed sea clutter using an incoherent surveillance radar, detecting the envelope of the backscattered amplitude. They documented that sea clutter fluctuates rapidly from pulse to pulse and is modulated by an underlying structure. The modulating structure fluctuates in the order of a few seconds and can be identified as the modulation of the radar cross section due to the

0-7803-4108-2/97/$10.00 ©1997 IEEE

ocean surface wave field. The fast fluctuating component having a decorrelation time scale of $5 - 10 \cdot 10^{-3}$ s results because many scatterers are contributing coherently to the backscatter from a resolution cell of the radar.
Because different resolution cells represent independent samples, a grainy appearance of radar images, called clutter noise, results. The sea clutter of marine radars with the two components was analyzed decades ago [*Croney*, 1966] with the intention to suppress the sea clutter, disturbing nautical applications.

3 General Principle of WaMoS

In contrast to nautical purposes WaMoS uses the sea clutter as a signal to analyze the spatio-temporal wave field (Fig. 1). Using this device it is now possible to sample time series of polar nautical radar images. The temporal sampling period, given by the antenna rotation period τ, is approximately two seconds. The number of the analyzed radar images is basically unlimited, but 32 are sufficient for operational purposes. From the polar images a rectangular area is chosen for spectral analysis. The gray levels in this area are setted on a cartesian grid using the nearest neighbourhood method. The grid size is chosen to be equal to the radar resolution of typically 10 m. The analyzed area having the size of approximately 1 km × 2 km should be placed as close to the antenna as possible to have an azimuthal overlap of 180°. This is necessary to get the full spectral information of the surface wave field because azimuthal traveling waves are not imaged by radars. The spatio-temporal information of the radar backscatter is transformed using a three dimensional Fast Fourier Transform (FFT) to the wavenumber frequency spectral space. This method gives reliable results if the analyzed area of sea surface is statistically homogeneous, and stationary during the measurement time. The image power spectrum $\mathcal{I}(\vec{k}, \omega)$ is mirror symmetric to the coordinate's origin. The spectral energy of the surface wave field is localized on a surface in the wavenumber frequency space (dispersion shell), because the frequencies and wavenumbers of the surface waves are connected by the dispersion relation (Fig. 2). The modulation signal of the wave field is correlated between adjacent images. On the other hand, the clutter component is uncorrelated and therefore spectrally white. The localization of the modulation signal on the dispersion shell enables the separation from the clutter noise pedestal, which is not possible if the spectral information of the sea state is extracted from a single radar image.

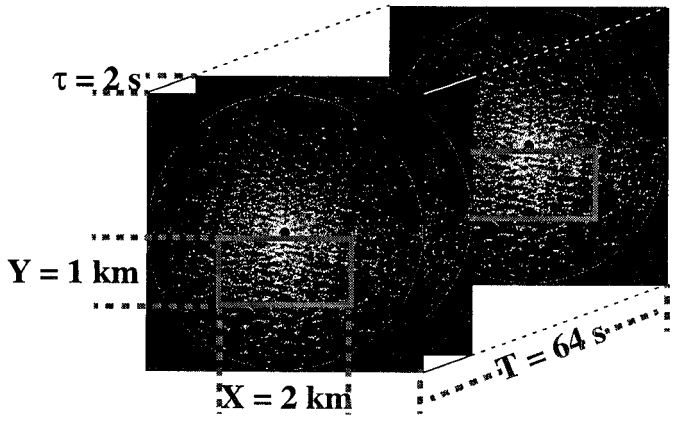

Figure 1: WaMoS digitize image sequences of a nautical radar. The rectangular area is used for the analysis of the spatio-temporal wave pattern.

4 Structure of the Wavenumber Frequency Spectra

In this section it is shown that the structure of the wavenumber frequency spectrum can be deduced from the dispersion relation, the aliasing effect, and the nonlinearity of the imaging process.

4.1 Linear surface gravity waves

The absolute frequency ω of linear surface gravity waves depends on the wavenumber $\vec{k}$, the water depth d and the velocity of encounter $\vec{U}_e$ between the sensor (radar) and the water body, which is the vector sum of the ship's speed over ground and the near surface current velocity. This dependency, expressed by the dispersion relation $\omega_a = \varpi_O^+$, is given by

$$\varpi_0^+(\vec{k}, d, \vec{U}_e) = \sigma_0^+(k, d) + \omega_D(\vec{k}, \vec{U}_e), \qquad (4.1)$$

with the intrinsic frequency

$$\sigma_0^+(k, d) = \sqrt{gk \cdot \tanh kd} \qquad (4.2)$$

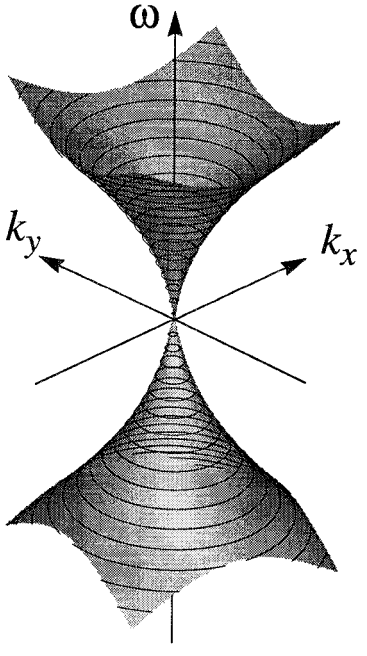

Figure 2: The dispersion shell in the wavenumber frequency spectral space.

and the Doppler frequency

$$\omega_D(\vec{k}, \vec{U}_e) = \vec{k} \cdot \vec{U}_e. \tag{4.3}$$

Only the solution of the dispersion relation with the positive square root, indicated by the + sign, has to be taken into account. This solution contains the full spectral information of the wave field because of the mirror symmetry to the origin of the spectral coordinates

$$\mathcal{I}(\vec{k}, \omega) = \mathcal{I}(-\vec{k}, -\omega) \tag{4.4}$$

(fig. 2). The absolute frequency may become negative due to a large negative Doppler shift when the sensor's platform moves faster than the phase speed of the waves.

4.2 Aliasing in the Frequency Domain

The full spectral information of an image sequence is contained in the frequency interval $0 \leq \omega \leq \omega_{Ny}$. The Nyquist frequency ω_{Ny} is given by $\omega_{Ny} = \pi/\tau$, where τ is the antenna rotation period. If the waves are temporally undersampled (less than twice each period, i.e. the Nyquist frequency is exceeded) the aliasing effect occurs. Aliasing in the frequency domain results in a $2\,\omega_{Ny}$-periodicity

$$\mathcal{I}(\omega) = \mathcal{I}(\omega + n \cdot \omega_{Ny}) \tag{4.5}$$

of the spectral space, in addition to the mirror symmetry to the origin of the spectral coordinates (4.4). With these symmetries, it is possible to reconstruct the original dispersion shell from the spectral energy mapped into the frequency interval $0 \leq \omega \leq \omega_{Ny}$ [*Seemann and Ziemer*, 1995]. The procedure is illustrated in Fig. 3 for the frequency interval $-\omega_{Ny} \leq \omega \leq 3\,\omega_{Ny}$. The sampling theorem is not violated in this context because the dispersion relation as additional physical information is used for the unambiguous reconstruction of the spectrum. The reconstruction is especially important for ship based nautical radars, resulting in a large Doppler shift due to the ship's speed, and for short waves in fetch limited coastal areas (Fig. 4).

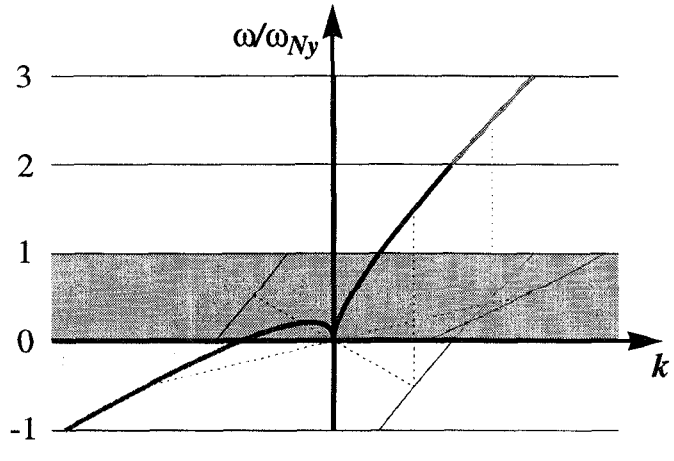

Figure 3: k-ω slice of a dispersion shell, illustrating the reconstruction procedure. The procedure utilizes the $2\ \omega_{Ny}$-periodicity and mirror symmetry to the origin to defold the dispersion shells from the original frequency interval $0 \leq \omega \leq \omega_{Ny}$ (gray box).

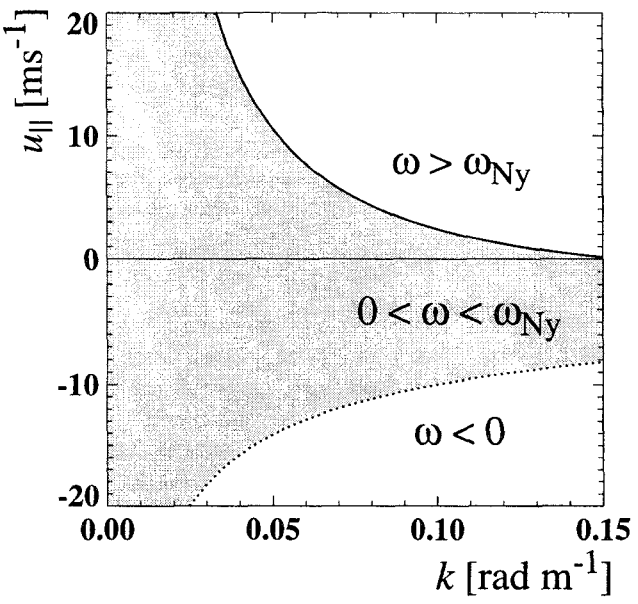

Figure 4: The limits of the operational WaMoS algorithms for the component of the velocity of encounter parallel to the wave propagation direction $u_{||}$ and the wavenumber k. The limits have been overcomed with the reconstruction procedure [*Senet*, 1996].

4.3 Nonlinear Imaging of the Surface Waves

Shadowing is assumed to be the dominant modulation mechanism at grazing incidence. It is supposed that shadowing can be treated with geometric (ray-) optics for HH-polarization. This is confirmed by numerical calculations of diffraction in the geometric shadowed portions of a wave profile [*Barrick*, 1995].

For a single wave at the ocean surface and the approximation of uniform grazing angle, the image spectrum of the geometric shadow mask can be given analytically. Figure 5 shows a sine wave, the shadow mask, and it's image spectrum. The spectral peak at the wavenumber k_0 is termed the fundamental (linear) mode and the peaks at integer multiples of k_0 the harmonic (nonlinear) modes of the image spectrum.

It is not possible to give an analytical function for the shadow mask of a surface wave field, consisting of the superposition of many partial waves. Therefore a simulation of the ocean surface wave field along with the calculation of the shadow mask was used for the examination of the imaging properties of shadowing.

Fig. 6 illustrates the coupling of two partial waves due to the nonlinearity of the imaging process. Spectral energy at sum and difference coordinates, as well as harmonics are obtained. This was verified using simulated and measured spectra of a crossing sea. The harmonics are localized at integral multiples of the fundamental mode coordinates:

$$(\vec{k}_p, \omega_p) = (p+1) \cdot (\vec{k}_0, \omega_0). \tag{4.6}$$

The index p indicates the p-th harmonic. The harmonics are localized on scaled dispersion shells.

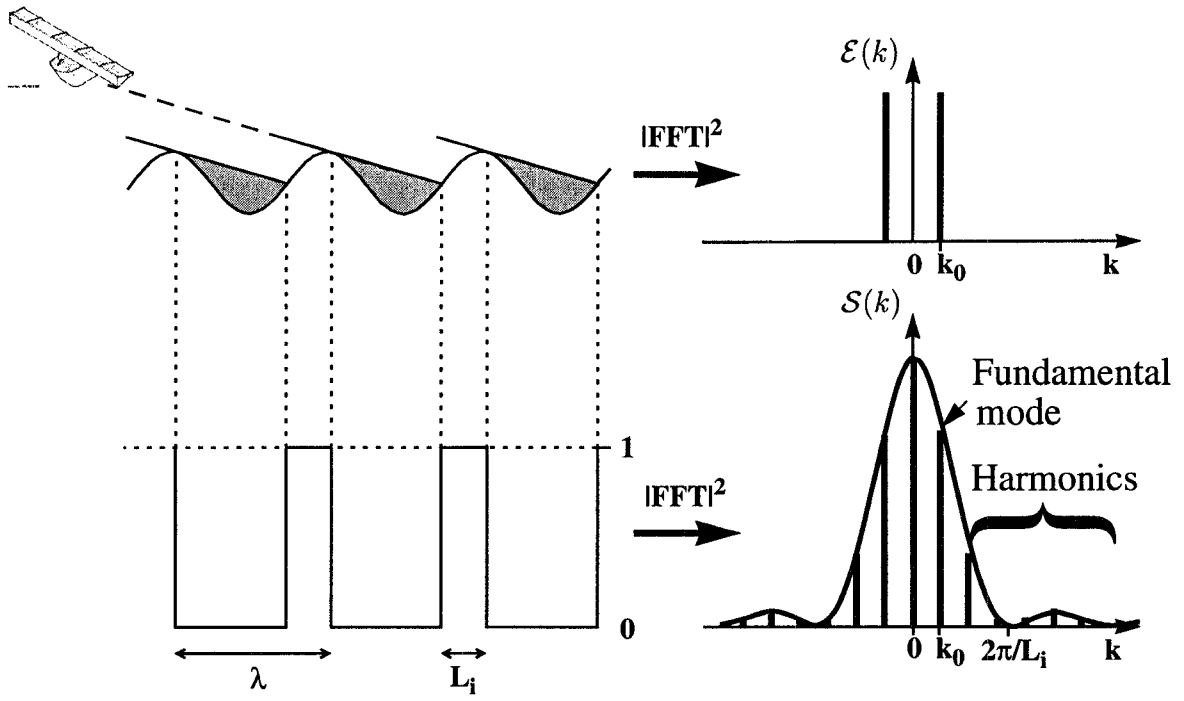

Figure 5: Shadowing as a nonlinear imaging process, illustrated for a sine wave.

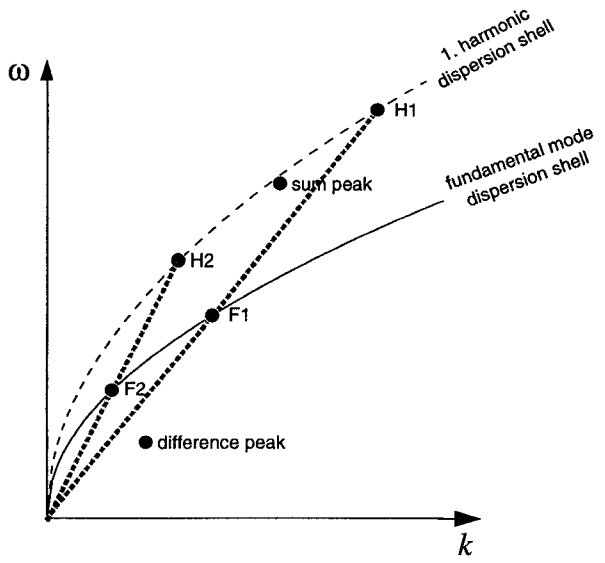

Figure 6: Nonlinear signal structure, illustrated with a k-ω slice of the image spectrum.

4.4 Impulse Response of the Radar

In the wavenumber domain aliasing is avoided because each spatial sample represents the averaged radar cross section of a resolution cell. This spatial averaging is equivalent to low-pass filtering in the wavenumber domain, suppressing aliasing. This effect is expressed by the radar's impulse response function. The impulse response can be analyzed directly with the radar data. Fig. 7 shows a wavenumber slice of the wavenumber frequency spectrum at a constant frequency, with the spectral energy at the intersections with the dispersion shells removed. The white clutter noise spectrum shows a cutoff to higher wavenumbers due to the weighting with the impulse response function. The elliptical shape of the clutter spectrum results because the azimuthal resolution is higher than the radial resolution. For higher wavenumbers a correction of the image spectrum is necessary. In the frequency domain the duration of the radar backscatter measurement of a resolution cell is negligible compared with the antenna rotation period,

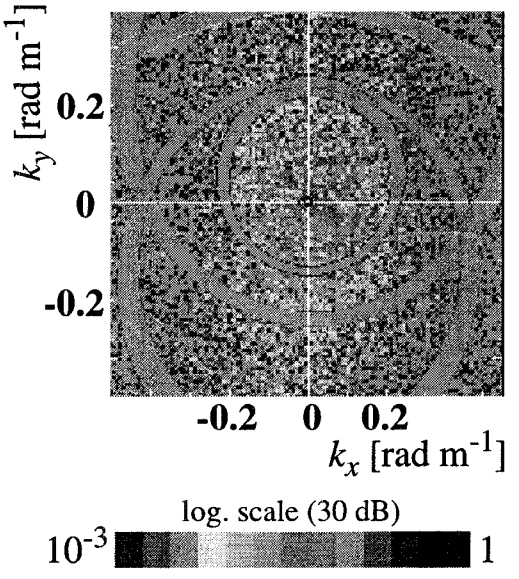

Figure 7: The effect of the radar's impulse response on the clutter spectrum, demonstrated with a k_x-k_y-slice of the image spectrum. The spectral energy at the intersections with the dispersion shells is removed.

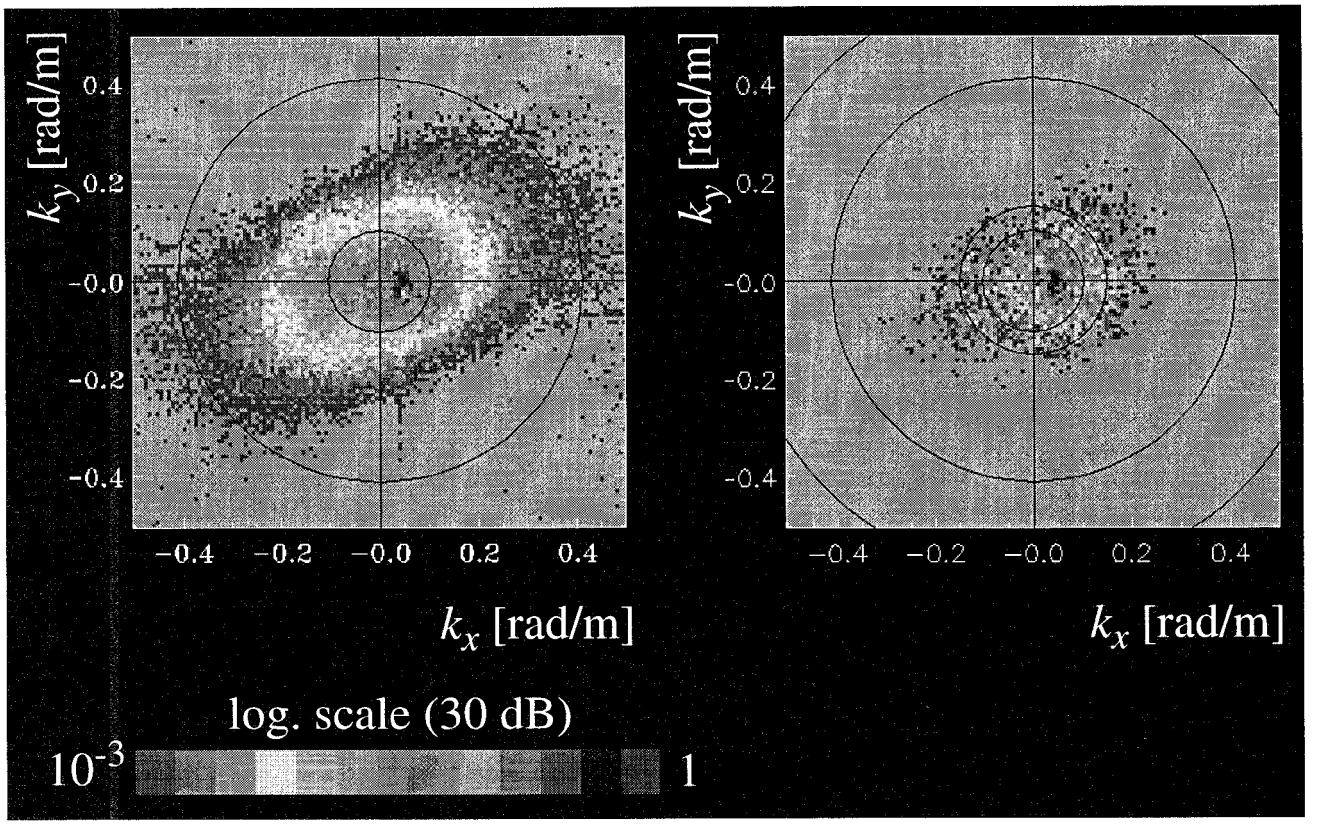

Figure 8: Reduction of the clutter noise pedestal with the spectral filter method. Integrated wavenumber image spectrum without spectral filtering (left) and the low noise filtered spectrum (right).

and aliasing occurs.

5 Spectral Filter Method

With the velocity of encounter and the water depth in shallow waters known as accurately as possible, the dispersion shell is used as a signal filter to select the spectral information of the sea state from the noisy wavenumber frequency image spectra. A least square method to determine the velocity of encounter at known water depth, taking into account the harmonic dispersion shells and the aliasing effect, is described by *Senet* [1996] and *Senet et al.* [1997]. The filter procedure starts with the reconstruction of the dispersion shell $\varpi_0^+(\vec{k}, d, \vec{U}_e)$ from the spectral energy folded into the frequency interval $0 \leq \omega \leq \omega_{Ny}$. Integration over the frequency coordinate axis

$$\mathcal{I}^+(\vec{k}) = 2 \cdot \int_{\omega=-\infty}^{\infty} \mathcal{I}(\vec{k}, \omega)\, \delta[\omega - \varpi_0^+(\vec{k}, \vec{U}_e)]\, d\omega \qquad (5.7)$$

results in a two-dimensional wavenumber spectrum. The δ-function corresponds to the dispersion shell, used as a signal filter. The wavenumber spectrum $\mathcal{I}^+(\vec{k})$ is not 180°-ambiguous like the wavenumber spectrum calculated from a single image because the positive solution of the dispersion relation is selected, and the negative solution skipped. The factor 2 in (5.7) takes into account the spectral energy of the negative solution. Figure 8 shows the strong reduction of the clutter noise pedestal using the spectral filter method. The requirement of the reconstruction of the dispersion shell for a ship borne WaMoS is outlined in Fig. 9. The image spectrum presented was calculated from a measurement on a ship cruising at a speed of $U_e = 4.2$ ms^{-1}.

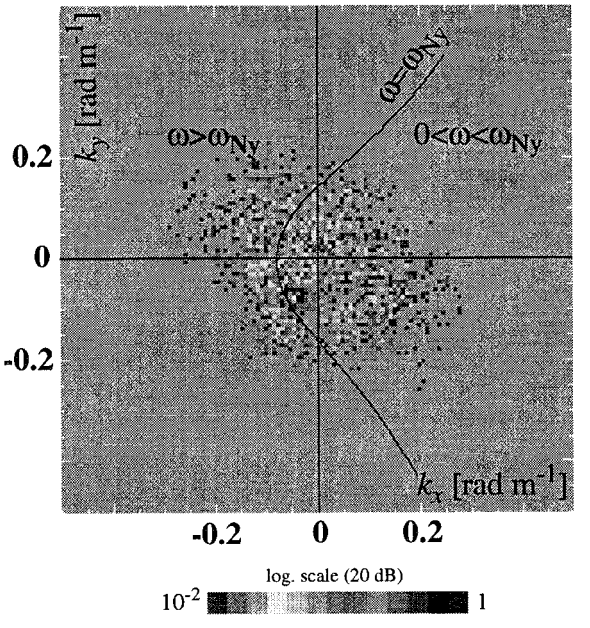

Figure 9: Integrated wavenumber spectrum measured with a ship borne WaMoS. The left portion corresponds to aliased energy and is selected with the reconstruction procedure.

Even in case of this moderate ship speed due to the Doppler frequency shift the shorter approaching waves are aliased, and can not be measured without the reconstruction.
The spectral amplitudes of the ocean wave spectrum $\mathcal{E}^+(\vec{k})$ (the variance spectrum of surface heave) are connected to the amplitudes of the image spectrum $\mathcal{I}^+(\vec{k})$ (the variance spectrum of gray levels) by an image transfer function, which is parameterized as a power law:

$$\begin{aligned} \mathcal{I}^+(\vec{k}) &= \alpha \cdot |\vec{k}|^\beta \cdot \mathcal{E}^+(\vec{k}), \\ \beta &\approx 1.2. \end{aligned} \tag{5.8}$$

The comparison with buoy measurements shows, that the value 1.2 for the exponent β is stable under a wide range of environmental conditions [*Ziemer and Rosenthal*, 1993]. The image transfer function is not azimuthal dependent because the rectangular area of the polar radar images chosen for the spectral analysis has an overlap of azimuth angles of the waves as close to 180° as possible.

6 Calibration Method

Using the spectral filter method, a series of 33 measurements having 5 minute time distance from the German research vessel GAUSS, was partitioned, selecting the spectral components. During the measurement period the significant wave height was approximately constant 3.5 m. Table 1 shows the distribution of the spectral energy in the different components of the image spectra. The image spectra are dominated by the clutter component, showing the importance of the spectral filter method to obtain low noise wavenumber spectra (Fig. 8). *Ziemer* [1995] found a correlation of the ratio of the peak energy $\mathcal{I}(\vec{k}_p, \omega_p)$ to the energy $\mathcal{I}_N$ not localized on the fundamental mode dispersion shell (the clutter and nonlinear signal components), with the significant wave height:

$$Hs = a + b \cdot \sqrt{\frac{\mathcal{I}(\vec{k}_p, \omega_p)}{\mathcal{I}_N}}. \tag{6.9}$$

After a calibration period, where the regression variables a and b are determined by comparing the radar data with an independent calibrated heave sensor, WaMoS can be used as a stand alone wave measuring device (Fig. 10). The determination of the significant wave height corresponds to the fixation of the calibration constant α in (5.8). The method does not require an absolute (radiometric) calibration of the radar images and is therefore especially useful

Spectral Component	Rate
Fundamental mode	0.341
1. Harmonic	0.077
Clutter noise	0.583

Table 1: Distribution of the spectral energy to the components.

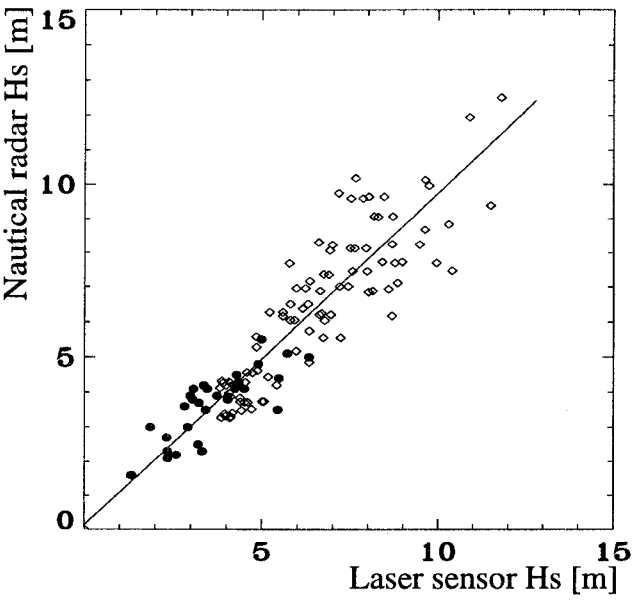

Figure 10: Comparison of the significant wave height measured with WaMoS and a laser heave sensor on an offshore platform in the Norwegian Ekofisk field, november and december 1994 (• calibration period, ○ independent measurements).

for a nautical radar. According to Table 1, the spectral energy $\mathcal{I}_N$ is dominated by the clutter component. The portion of the nonlinear signal structure's energy is negligible in the context of the calibration. The empirical calibration procedure has the same physical background as a method *Alpers and Hasselmann* [1982] proposed to calibrate SAR image spectra, based on the determination of the signal to noise ratio. The metdod works because the variance of the clutter noise pedestal and the modulation signal are measured in the same unit of radar backscatter, and the clutter noise pedestal can be used as a gauge of the energy scale.

7 Conclusions

The work outlined in this paper consisted of extending the applicability of the WaMoS analysis algorithms. Based on the clarification of the structure of wavenumber frequency spectra, the spectral filter method was supplemented with the reconstruction of the dispersion shell. The extended filter method enables the measurement of low-noise, unambiguous wavenumber spectra under short fetch conditions in coastal areas and on cruising ships using WaMoS. The physical background of the empirical calibration method has been clarified. Already in progress is the transfer of the improved algorithms to the operational WaMoS analysis software.

Acknowledgments

This work was carried out in the frame of the projekt SARPAK (BMBF No. 03F0165C). The authors owe thank to Dr. Nieto Borge (Clima Marítimo), whose simulation

software was used for this work.

References

Alpers, W., D.B. Ross, and C.L. Rufenach, On the Detectability of Ocean Surface Waves by Real and Synthetic Aperture Radar, *Journal of Geophysical Research*, Vol. 86, No. C7, pp. 6481-6498, 1981.

Alpers, W., and K. Hasselmann, Spectral Signal to Clutter and Thermal Noise Properties of Ocean Wave Imaging Synthetic Aperture Radars, *International Journal of Remote Sensing*, Vol. 3, No. 4, pp. 423-446, 1982.

Barrick, D.E., Near-Grazing Illumination and Shadowing of Rough Surfaces, *Radio Science*, Vol. 30, No. 3, pp. 563-580, 1995.

Croney, J., Improved Radar Visibility of Small Targets in Sea Clutter, *The Radio and Electronic Engineer*, Vol. 32, pp. 135-148, 1966.

Dittmer, J., Use of Marine Radars for Real Time Wave Field Survey and Speeding Up the Transmission / Processing, Proceedings of the WMO/IOC Workshop on Operational Ocean Monitoring using Surface Based Radars, Geneva, Report No. 32, pp. 133-137, 1995.

Lee, P.H.Y., J.D. Barter, K.L. Beach, C.L. Hindman, B.M. Lake, H. Rungaldier, J.C. Shelton, A.B. Williams, R. Yee, and H.C. Yuen, X Band Microwave Backscattering from Ocean Waves, *Journal of Geophysical Research*, Vol. 100, No. C2, pp. 2591-2611, 1995.

Magnusson, A.C., Operational Use of Marine Radar Information in Wave Forecasting; Status and Future Aspects, Proceedings of the WMO/IOC Workshop on Operational Ocean Monitoring using Surface Based Radars, Geneva, Report No. 32, pp. 95-102, 1995.

Nieto Borge, J.C., First Experience with the Use of Marine Radar to survey Ocean Waves close to the Spanish Coast, Proceedings of the WMO/IOC Workshop on Operational Ocean Monitoring using Surface Based Radars, Geneva, Report No. 32, pp. 88-94, 1995.

Seemann, J., and F. Ziemer, Computer Simulation of Imaging Ocean Wave Fields with a Marine Radar, *Oceans Proceedings*, pp. 1128-1133, 1995.

Senet, C.M., Untersuchungen zur Bestimmung der oberflächennahen Strömungsgeschwindigkeit mit einem nautischen Radar, Diploma Thesis, University of Hamburg and GKSS Research Center, GKSS-Report 97/E/3, 1996.

Senet, C.M., J. Seemann, and F. Ziemer, An Iterative Technique to Determine the Near Surface Current Velocity from Time Series of Sea Surface Images, *Oceans Proceedings*, 1997.

Trizna, D.B., R. Bachman, and M. Whalen, Remote Sensing of Ocean Wavenumber Spectra using Shipboard Marine Radar, *Oceans Proceedings*, pp. 67-72, 1995.

Ward, K.D., C.J. Baker, and S. Watts, Maritime Surveillance Radar Part 1: Radar Scattering from the Ocean Surface, *IEE Proceedings*, Vol. 137, Pt. F, No. 2, pp. 51-62, 1990.

Young, I.R., W. Rosenthal, and F. Ziemer, A Three-Dimensional Analysis of Marine Radar Images for the Determination of Ocean Wave Directionality and Surface Currents, *Journal of Geophysical Research*, Vol. 90, C1, pp. 1049-1059, 1985.

Ziemer, F., and W. Rosenthal, Measurement of Two-Dimensional Wave Energy Spectra during SAXON-FPN'90, *Oceans* , pp. II-326 - II-331, 1993.

Ziemer, F., An Instrument for the Survey of the Directionality of the Ocean Wave Field, Proceedings of the WMO/IOC Workshop on Operational Ocean Monitoring using Surface Based Radars, Geneva, Report No. 32, pp. 81-87, 1995.